11th International Workshop on Ship and Marine Hydrodynamics
Hamburg, Germany, September 22-25, 2019

A Computational Study for Flow past a Junction with a Strake

You-Sheng Lin[1], Jiahn-Horng Chen[1,*]

[1]National Taiwan Ocean University, Department of Systems Engineering and Naval Architecture
2 Pei-Ning Road, Keelung 20224, Taiwan

*Corresponding author, b0105@mail.ntou.edu.tw

ABSTRACT

A strake is a practice device to install in front of a wing-body junction to suppress horseshoe vortex. In this paper, we designed a strake for a finite wing mounted on a flat plate. Its profile on the plane of symmetry is an ellipse. The horizontal cross sections of the strake are also elliptical. The flow due to a flat plate boundary layer passing the wing with zero angle of attack was studied computationally.

Some sets of values of the strake length and height were chosen for study. The flow was first studied computational via RANS equations. The solutions which show no horseshoe vortex were then picked. Then the LES computations were employed to investigate the detailed flow characteristics. The solution by RANS computations represents the time-averaged one and that by LES computations depicts the instantaneous features of the flow. Some interesting features not revealed in RANS computations were found in LES computations.

1 INTRODUCTION

The wing-body junction flow have been widely studied. Early investigations mainly came from aerospace industry. The flow is non-planar and difficult in theoretical analysis [1]. The experiment shows that vortices are formed due to separation of the boundary layer on the body in the flow towards the wing. The free edge of the resulting vortex sheet rolls up to form the vortex which then trails downstream around the wing [2]. The horseshoe vortex has been identified. In addition, it was found that the drag could substantially increase [3].

More detailed physical phenomena and flow structures were subsequently found and analysed with more experiments being conducted and flow observations. The generation of secondary flow (horseshoe vortical flow) in the wing-body junction is due to the lateral skewing of the shear layer, rather than the Reynolds-stress gradients. It has been known that the Reynolds-stress-induced secondary flows are slow to develop and the skew-induced secondary flows are slow to be attenuated by Reynolds stresses [4]. The slow attenuation of horseshoe vortex may result in wide-region influence on the downstream flow development. For examples, the vortices created at the sail/submarine-body junction may induce effects on control surface and propeller operations when vortices are carried downstream. Scouring appears in the nose region of a bridge pier when the non-planar vortices pass around it.

In addition, these vortices are highly unsteady and, hence, induce high turbulence intensities and surface pressure fluctuations [5]. The characteristics of unsteadiness have been extensively investigated. The typical flow around the wing-body junction formed by a 3:2 semi-elliptic nose/NACA 0020 tail section and a flat plate was the target in many studies. Fleming *et al*. examined the effects of the approaching boundary-layer flow on the junction flow [6]. They compared their experimental results with other data of the same body shape and found that the momentum deficit factor was an important factor for the mean flow distortion magnitudes and vorticity distribution. Devenport and Simpson showed in their experiment that the horseshoe vortex system exhibited bimodal, low-frequency random oscillations [7]. Paik *et al*. also found this physical phenomenon by LES computations [8]. Their explained from their computational results that the bimodal

dynamics was due to the continuous and aperiodic interplay of two basic states: “an organized state with a coherent necklace-like horseshoe vortex, and a disorganized state with hairpin vortices wrapping around it.” Gand *et al*. observed that the bimodal behaviour was characterized by multiple frequencies with the Strouhal number, based on the boundary-layer thickness one-half chord upstream the wing, ranging from 0.05 to 0.1 [9]. Due to the bimodal phenomenon, the core of the horseshoe vortex oscillates around its mean location.

There are also studies of effects due the wing-body geometry on the junction flow development. Among them, Mehta’s experiments showed that the size and strength strongly depended on the wing nose shape; they increased with the nose bluntness [10]. Later, Ö lçmen and Simpson also had similar observations in their LDV experiment [11]. The LDV measurements by Ahmed and Khan indicated that the vortex moved towards the wing for back sweep and away for the forward sweep [12]. In addition, many investigations were devoted to mitigating the horseshoe vortex by some kind of additional small structures. The review paper by Beg and Beg [13] presented several types of flow altering devices in the vicinity of pier to reduce scour which is a direct consequence of horseshoe vortex. Devenport *et al*. [14-15] introduced a leading-edge strake to modify the incoming flow and eliminate flow separation upstream leading edge. This approach has its best effect when the incoming flow has a zero angle of attack. Wang *et al*. [16] proposed an upstream inclined rod to mitigate the horseshoe vortices for a circular cylinder mounted on a flat plate. They showed that the adverse pressure gradient on the flat plate upstream of the cylinder was significantly reduced and the pressure fluctuations in the vicinity of the cylinder were attenuated. Kang *et al*. [17] investigated the effect of an upstream cavity on the horseshoe vortices around a circular cylinder. They concluded that the strength of the primary vortex was weakened because of the fluid stream engulfed in to the cavity which resulted in mainstream diffusion. Theberge and Ekmekci [18] studied the effects of an upstream triangular plate on the mitigation of horseshoe vortex. This could be simplest structure ever devised for the purpose to suppress horseshoe vortices. Their study concluded that the longer and thinner the plate was, the better the vortex mitigation was. In fact, this conclusion is similar to that of employing a strake [19].

In this study, we designed a simple strake. Its horizontal cross section is part of ellipse. Some sets of values of the strake length and height were chosen for study. The flow was first studied computational via RANS equations. The solutions which show no horseshoe vortex were then picked. And then the LES computations were employed to investigate the detailed flow characteristics. The solution by RANS computations represents time-averaged one and that by LES computations depicts the instantaneous features of the flow. The comparison will be presented in the paper.

2 THE PHYSICAL DESCRIPTION OF FLOW PAST A WING WITH A STRAKE

A strake is a practice device to install in front of a wing-body junction to mitigate horseshoe vortex. We study the flat-plate boundary layer flow past a wing with a strake at its leading edge. The wing is vertically mounted on the flat plate and its span is finite, as shown in Figure 1. The origin of the Cartesian coordinate system is at the leading edge of the wing on the flat plate, with the *x*-axis in the streamwise direction, *y*-axis in the spanwise direction, and *z*-axis in the cross-flow direction. The flat plate boundary layer passes the wing with zero angle of attack.

Shown in Figure 2(a), the wing section is composed by a 3:2 ellipse and the NACA 0020 section. They join together at the maximum thickness. The profile of the strake on the plane of symmetry is a

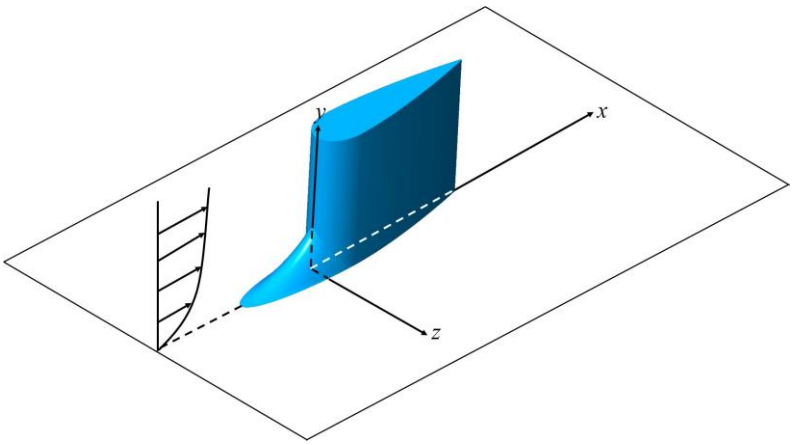

Figure 1: Schematic of flow past a wing with a strake.

generalized ellipse as shown in Figure 2(b), in which L and H represents the length and height of the strake, respectively. The horizontal cross sections of the strake are shown in Figure 2(c). The one on the flat plate is described as a part of another ellipse as shown. The cross section at $y > 0$ is of the same form as the one on the flat plate but is shifted rightwards so that the left vertex coincides with the generalized ellipse described in Figure 2(b).

The flow is governed by the incompressible Navier-Stokes equations which can be expressed in the tensor form as

$$\frac{\partial u_i}{\partial x_i} = 0 \tag{1}$$

$$\rho \frac{\partial u_i}{\partial t} + \rho u_j \frac{\partial u_i}{\partial u_j} = -\frac{\partial p}{\partial x_i} + \mu \frac{\partial^2 u_i}{\partial x_j \partial x_j} \tag{2}$$

where ρ is the density of fluid, p the static pressure, μ the dynamic viscosity, $(x_1, x_2, x_3) = (x, y, z)$ the coordinate system, and $(u_1, u_2, u_3) = (u, v, w)$ the velocity field.

The Reynolds-averaged Navier-Stokes (RANS) equations can be obtained by averaging the Navier-Stokes equations in time and are given by

$$\frac{\partial \overline{u_i}}{\partial x_i} = 0 \tag{3}$$

$$\rho \frac{\partial \overline{u_i}}{\partial t} + \rho \overline{u_j} \frac{\partial \overline{u_i}}{\partial x_j} = -\frac{\partial \overline{p}}{\partial x_i} + \frac{\partial}{\partial x_j}\left(\mu \frac{\partial \overline{u_i}}{\partial x_j} - \rho \overline{u_i' u_j'} \right) \tag{4}$$

where the terms with an overbar represent the time-averaged physical quantities and $\overline{u_i' u_j'}$ the Reynolds stresses. To make the equations closed for solution, we need to employ some kind of turbulence model. Here in this study, we used the Spalart-Allmaras one-equation model with rotation/curvature correction developed by Spalart and Shur [20] and Shur *et al*. [21]. This form of the Spalart-Allmaras model attempts to account for rotation and curvature effects.

Large eddy simulation (LES) is another popular technique for simulating turbulent flows. The equations solved for LES are obtained by a filtering rather than an averaging process. It is an inherently transient technique in which the large scales of the turbulence are directly solved for by a transient calculation and the small-scale motions are modelled by a subgrid-scale (SGS) model. There are several SGS

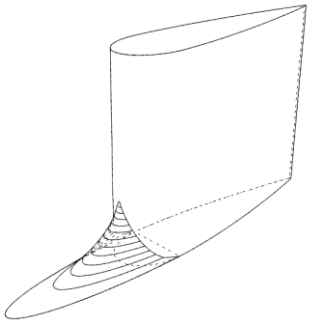

(a) Wing with a strake.

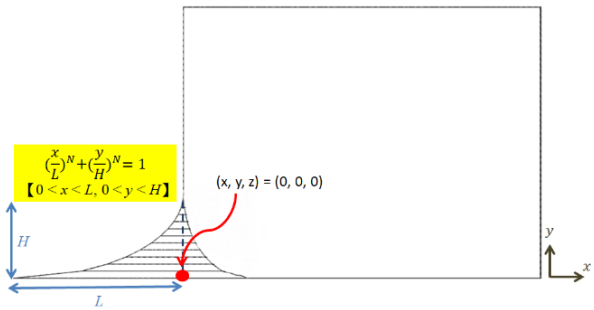

(b) Strake profile on the plane of symmetry.

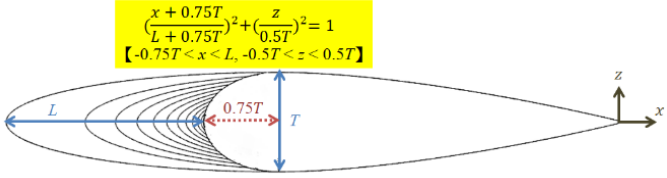

(c) Strake profile viewed from top.

Figure 2: The geometry of the wing-body junction with a strake.

models available. In our study, the dynamic Smagorinsky-Lilly (DSL) model [22-23] was employed. Its concept is to apply a second filter (called the test filter) to the equations of motion. Some constants to be determined in the SGS model are decided by the procedure proposed by Germano *et al*. [24] and Lilly [25].

In the present study, some sets of values of the strake length and height were chosen for investigation. The flow was first solved computational via RANS equations. The solutions which show no horseshoe vortex were then picked. Then the LES computations were employed to investigate the detailed flow characteristics in order to ensure whether the horseshoe vortices were mitigated. The solution by RANS computations represents time-averaged one and that by LES computations depicts the instantaneous features of the flow.

The computational domain is shown in Figure 3. The upstream boundary condition was specified with the boundary-layer velocity profile obtained by Devenport and Simpson [26] in their wind-tunnel experiments. As shown in Figure 3, this profile was prescribed upstream at $x = -18.2T$, where T represents the maximum thickness of the wing. The present study was conducted at the Reynolds number $Re = 5 \times 10^5$, based on the chord length of the wing. The commercial software ANSYS Meshing was employed for grid generation. A structured grid was generated around the wing body. Outside the structured grid was embedded with a non-structured polyhedral mesh. The total grid number is about 900 million. All computations were made using ANSYS Fluent. The region upstream of the leading edge was refined in order to capture the horseshoe vortex.

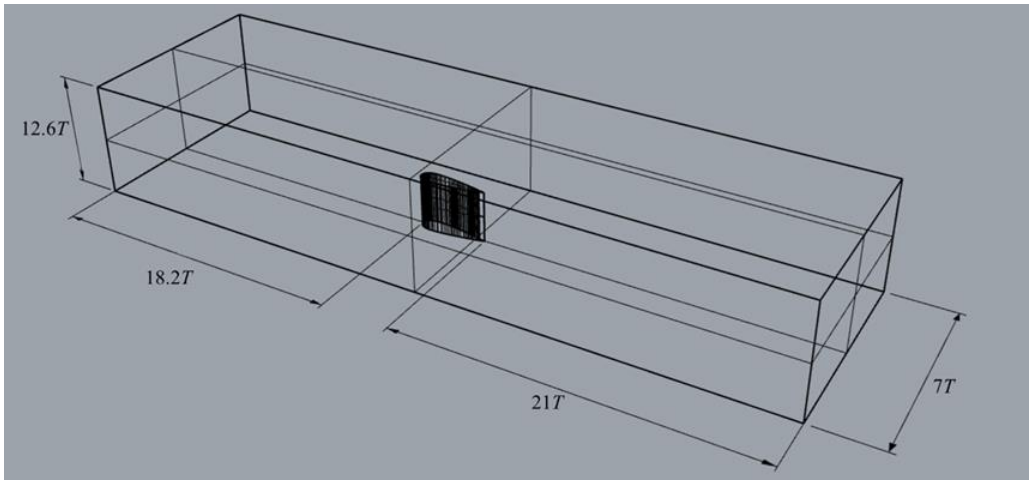

Figure 3: The computational domain.

3 RESULTS AND DISCUSSION

The result presentation and discussion will be divided into several parts. For the first part, we will first present the result without strake and compare with the available data in the literature. Then we will proceed to discussing the results for the wing with a strake of $L/H = 2$, where $L = 0.5T$ and $2T$.

3.1 Flow near the leading edge for the wing without a strake

Figure 4 shows the computational results by RANS equations and LES and the experimental data by Devenport and Simpson [7]. The results by RANS shown in Figure 4(a) exhibits a major vortex with center at around $(x/T, y/T) = (-0.29, 0.04)$, two minor vortices around the major one, and another minor one at the leading edge. For comparison, the experimental data show in Figure 4(c) show only one vortex with center at $(x/T, y/T) = (-0.20, 0.05)$. This could be due to the fact that measurement region by the LDV system did not cover the area very close to the flat plate and the leading edge. The location of the vortex core by computation is obviously farther away from the leading edge than that by experiment. Nevertheless, the computational results show satisfactory agreement with the experimental data. The plot by LES shown in Figure 4(b) is the time-averaged results which exhibit a multi-vortex system. The vortex system extends from $x/T = -1$ which is evidently far more upstream of the leading edge. The physics shown in the results by RANS seems quite different from those by LES. The LES results reveal more detailed vortical flow physics.

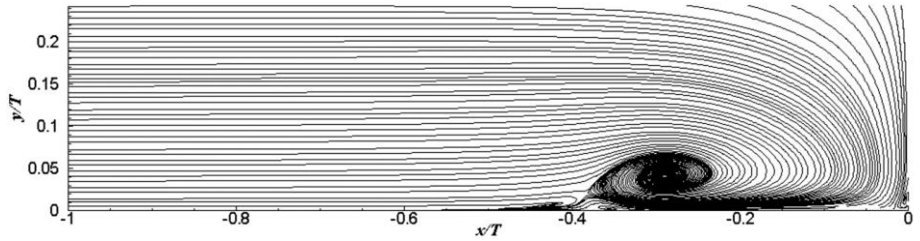

(a) Vortex system by RANS equations.

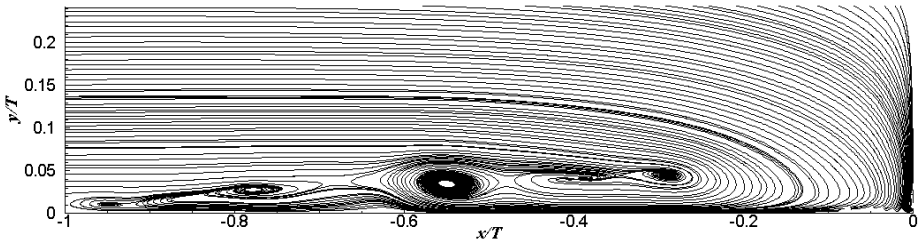

(b) Vortex system by LES.

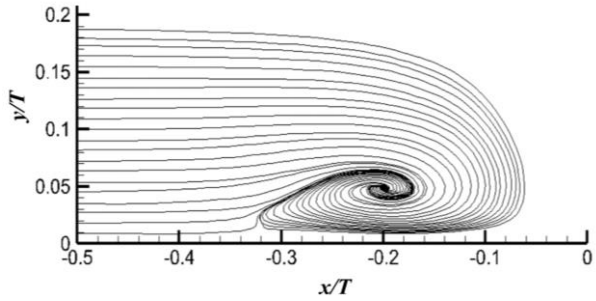

(c) Vortex system by experiment [7].

Figure 4: Vortex system on the symmetric plane.

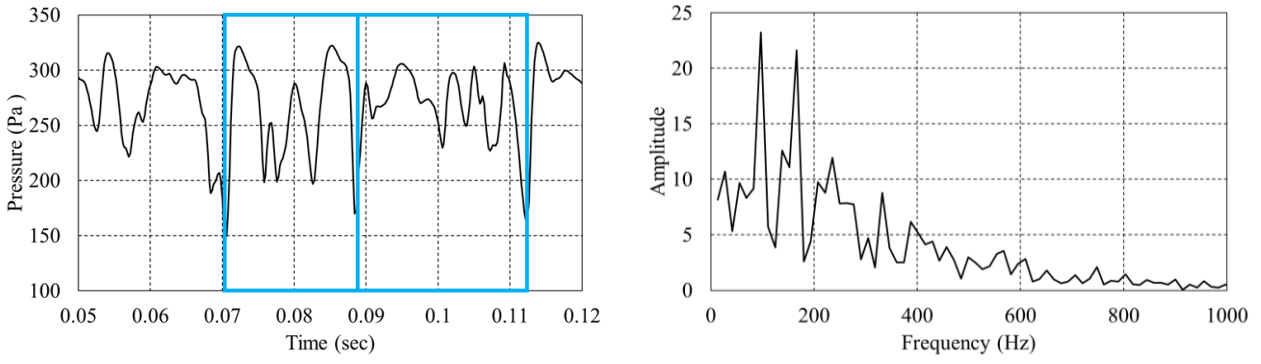

(a) Pressure variation with time.

(b) FFT analysis for the pressure.

Figure 5: Pressure fluctuation at $(x/T, y/T) = (-0.2, 0.05)$.

The flow revealed by LES are unsteady. These vortices move downstream and upstream aperiodically and experience amalgamation. Figure 5(a) shows part of the pressure fluctuation at $(x/T, y/T) = (-0.2, 0.05)$ where the vortex center is according to the experimental data. It is evident that the flow is not periodic shown in the FFT analysis in Figure 5(b). The two major frequencies are 97 Hz and 166 Hz. Furthermore, in Figure 5(a), we observed that the pressure fluctuation reaches once in a while its valleys which are less than 200 Pa. We may take these valley points as the rough interval division points for the vortical flow. Then in the plot, two intervals can be identified. It should be first noted that these division points do not represent the starting points or ending points of a periodic motion as we can easily find that the time spacing of these two intervals

are not equal and the pressure fluctuation patterns in these two intervals are totally different. However, they may be regarded as the starting point of vortical flow motion cycle which is not periodic.

In the following, we take the first interval (0.0704-0.0884 sec) to explain the oscillation of these vortices as shown in Figure 6. The process is divided into 11 stages from (a) to (k). At stage (a), the major vortex reaches at the observation point marked with "+" in the plot where (x/T, y/T) = (−0.2, 0.05). At this stage, the pressure reaches its minimum. At stage (b), the major vortex stagnates and amalgamates with the secondary vortex moving forwards with the flow into one. Then the amalgamated vortex moves upstream due to the adverse pressure gradient on the flat plate. This backward movement makes the pressure rise and reach a local maximum. Then the vortex moves forwards again and the pressure at the observation point decreases again. In the meantime, a new secondary vortex is created and moves downstream. At stage (d), the major vortex amalgamates with the new secondary vortex again when it moves forwards to the point at x/T = −0.2. Then at stage (e), the new vortex core moves a little upstream and makes the pressure at the observation point a little increase. Then another secondary vortex from upstream moves downstream at a higher speed with the major vortex as can be seen at stage (f). The secondary vortex reaches the major one and the two amalgamate into another new one which, again, moves upstream as shown at stage (g). This backward movement makes the pressure rise again. However, the major vortex soon changes its direction and move forwards up to x/T = −0.25 shown at stage (h). At this time, another secondary vortex amalgamates with the major one again into a stronger one at stage (i). This vortex moves downstream and the pressure at the observation point decreases at stage (j) till it reaches the observation point at stage (k).

It is observed that the process in a cycle consists of several creations and amalgamations of vortices and their forward-and-backward motion. The increase of pressure at the observation point indicates the backward movement of the vortices.

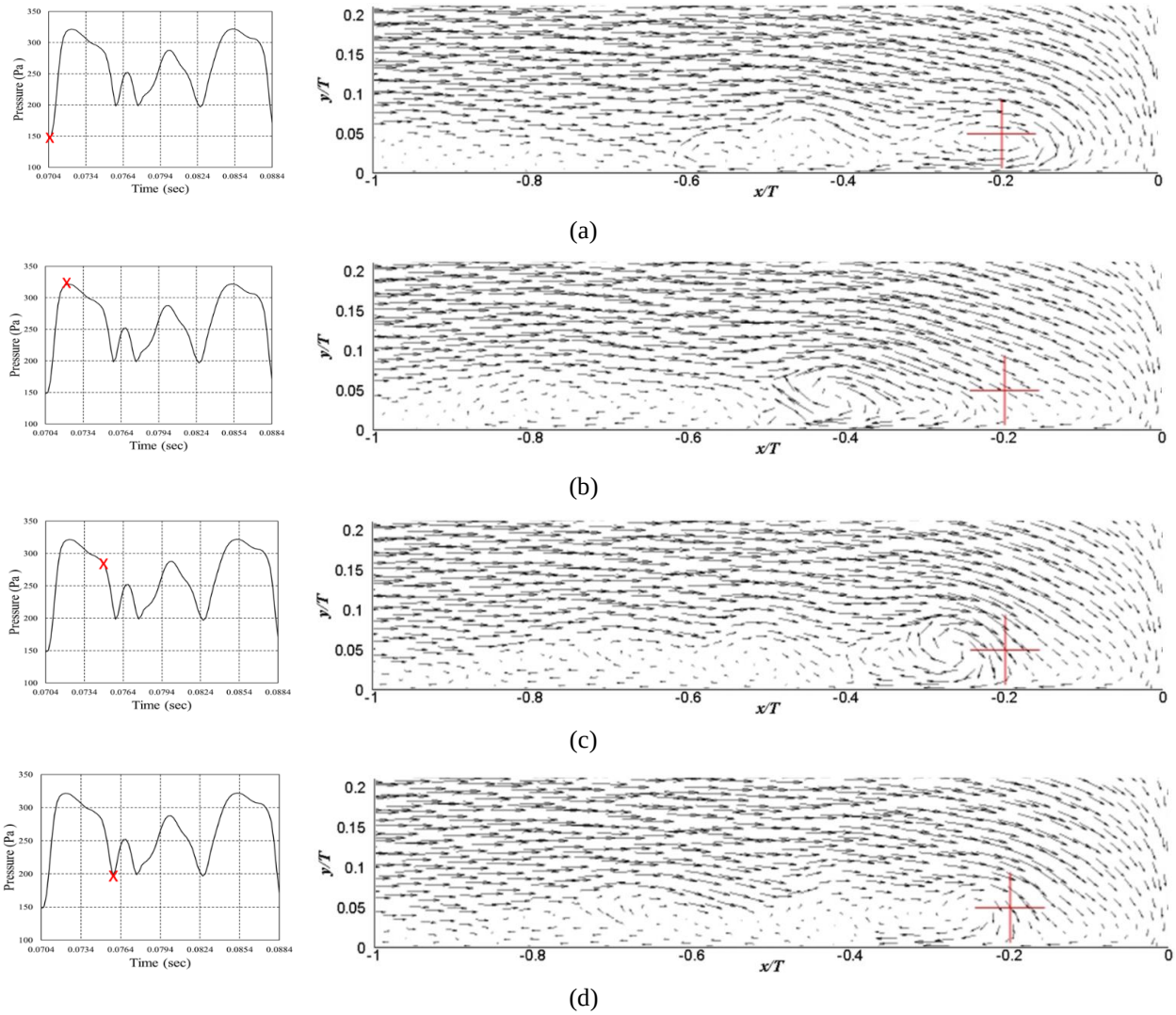

Figure 6: Motion of vortices and their amalgamation in a cycle.

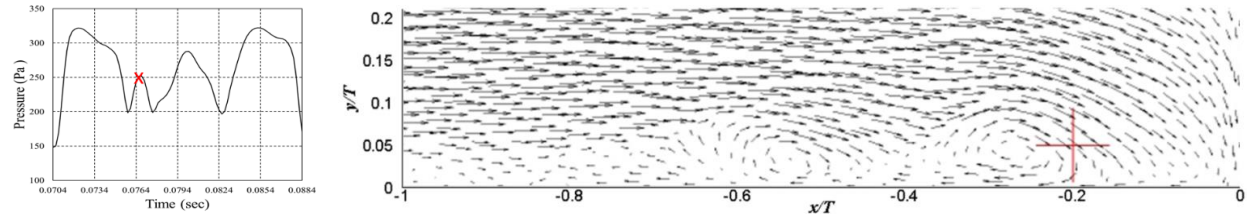

(e)

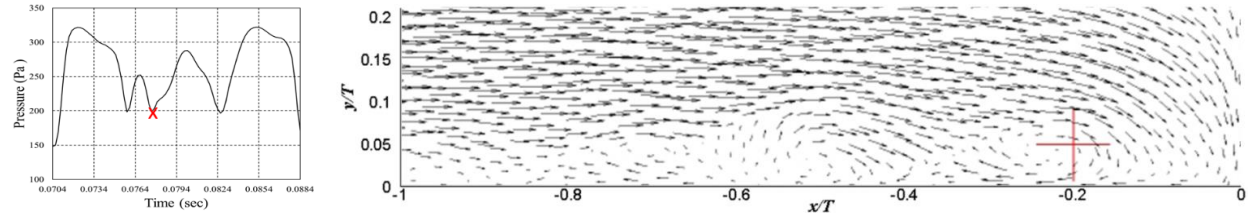

(f)

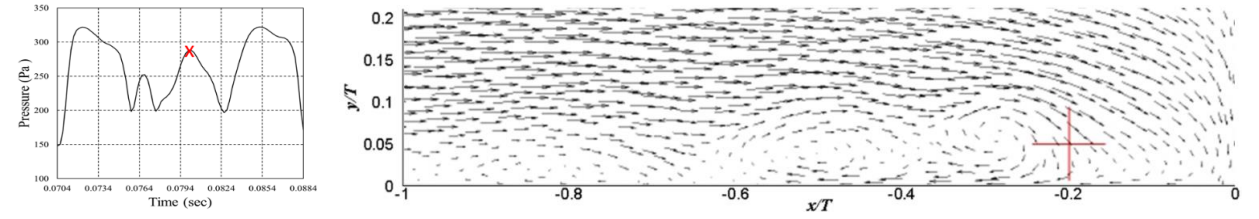

(g)

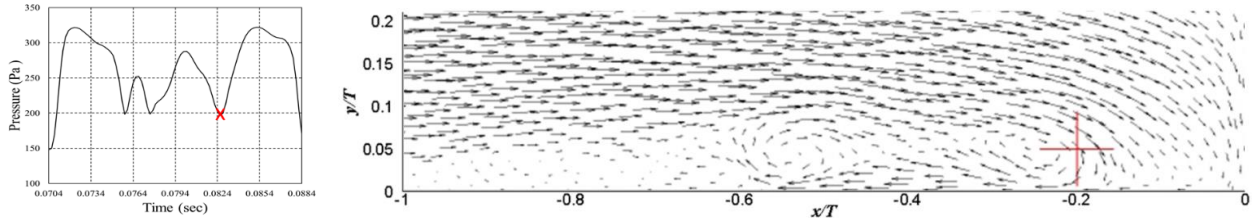

(h)

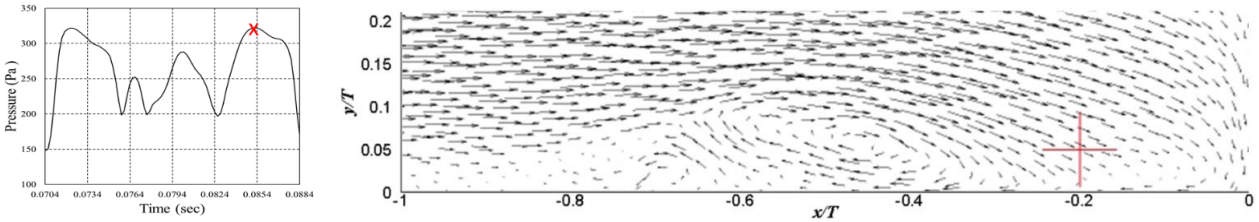

(i)

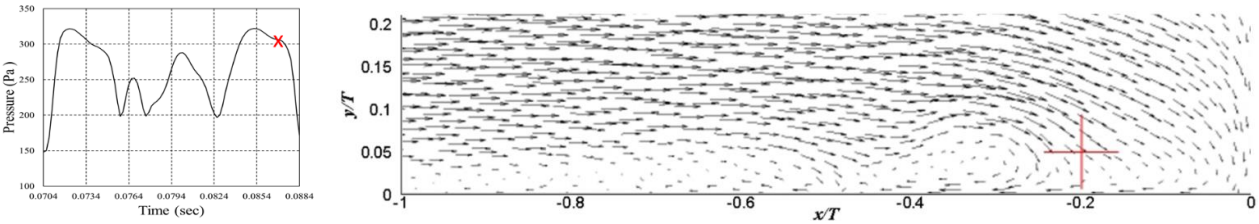

(j)

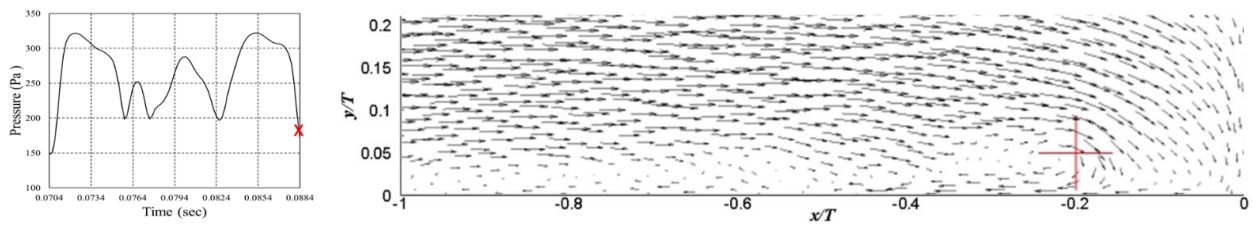

(k)

Figure 6: Motion of vortices and their amalgamation in a cycle (continued).

3.2 Flow near the leading edge for the wing with a short strake

Figure 7 shows the streamline patterns from the computational results by RANS equations and LES for the wing attached with a strake of length $L = 0.5T$. The results by RANS shown in Figure 7(a) exhibits a major vortex with center at around $(x/T, y/T) = (-0.33, 0.04)$. The vortex is above the strake surface. Obviously, the vortex is much smaller than that for the wing without strake shown in Figure 4(a). The addition of a short strake to the wing can reduce the strength of the horseshoe vortex but it is not fully mitigated in the RANS computation. Figure 7(b) shows the time-averaged results of LES computation. It also shows the existence of a small vortex which, however, is upstream of the strake.

Figure 8 exhibits the pressure fluctuation in time at $(x/T, y/T) = (-0.7, 0.01)$. In Figure 8(a), we find that the magnitude of fluctuation is reduced, compared to that in Figure 5(a). Indicated by the blue boxes, the fluctuation "cycle" apparently exists. The FFT analysis leads to the results shown in Figure 8(b). The main contributing frequency is about 80 Hz. Since there is only one major frequency, the bimodal fluctuation in the flow without a strake is suppressed when a strake is mounted. However, the flow in a cycle can vary significantly. In the blue intervals, the peak value of pressure is much larger than that in the red interval. Furthermore, the computation shows that when the major vortex moves downstream, it stagnates above the strake at about $x/T = -0.4$ for a short while. Then it moves up and forwards in the streamwise direction and elongates along the strake due to shearing effects. When it reaches at about $x/T = -0.28$, then it almost stagnates here, decays with time and finally disappears. This process is shown in Figure 9. Of course, the whole cycle consists of several creations and amalgamations of vortices.

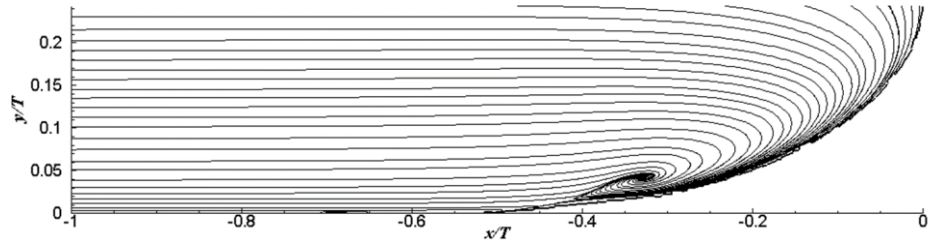

(a) Vortex system by RANS equations.

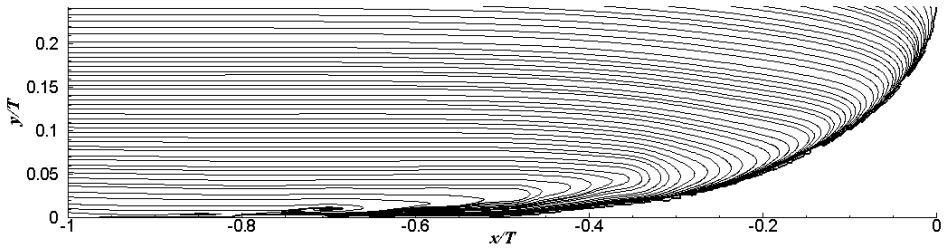

(b) Vortex system by LES.

Figure 7: Vortex system on the symmetric plane for the wing with a short strake.

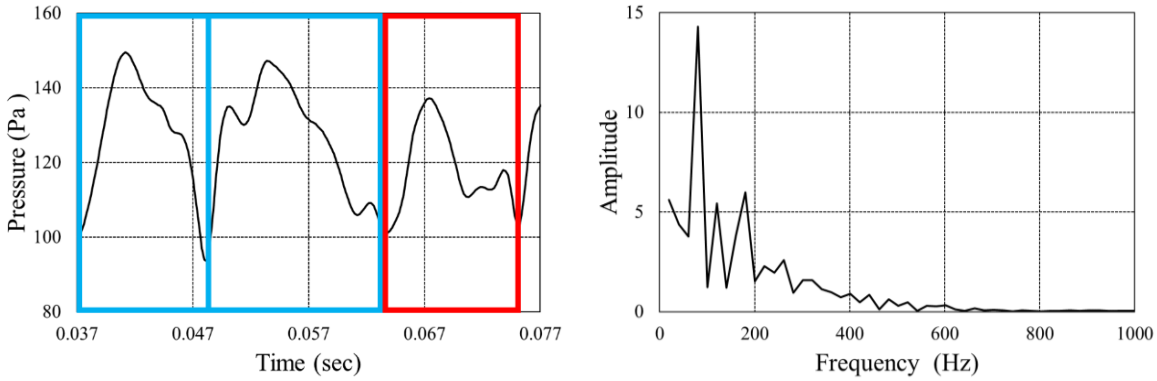

(a) Pressure variation with time.

(b) FFT analysis for the pressure.

Figure 8: Pressure fluctuation at $(x/T, y/T) = (-0.7, 0.01)$.

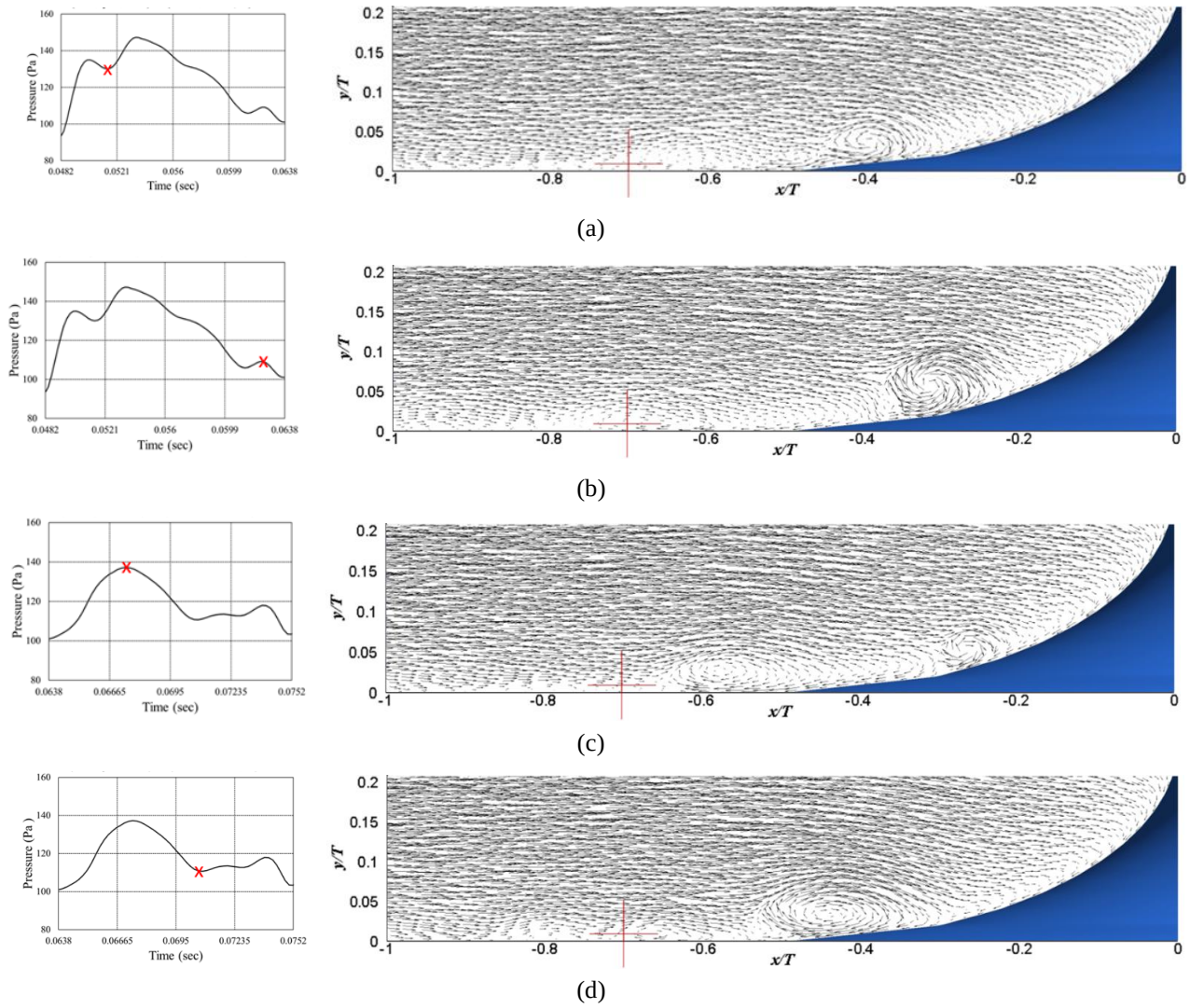

Figure 9: Motion of vortices and their amalgamation in a cycle for the wing with a short strake.

3.3 Flow near the leading edge for the wing with a long strake

Shown in Figure 10 are the computational results for the case with $L = 2T$ by RANS equations and LES. The results by RANS shown in Figure 10(a) exhibits no vortex system present in the flow field. It appears that the long strake can have better effect on the mitigation of the horseshoe vortex. This is consistent with other computational observation [19]. However, the time-averaged results by LES indicate that there exists a minute vortex as shown in Figure 10(b). Its center, $(x/T, y/T) = (-2.036, 0.004)$, is very close to the leading edge of the strake. It is so small that it could be ignored if the grid is not enough refined and the plot is not locally magnified. The computational results of the wing with these two strakes shown in Sections 3.2 and 3.3 infer that the strake length should be long enough to mitigate the horseshoe vortex. Furthermore, the results by RANS and LES are quite different in the sense that the vortex system could be different in terms of its distribution, strength, and location. However, the results from RANS computations could be enough to justify the existence of the horseshoe vortex.

In Figure 11, we plot the pressure fluctuation at $(x/T, y/T) = (-2.036, 0.004)$. In this LES computation, we identify the cyclic physical phenomenon as shown by the blue boxes in Figure 11(a). In each box interval, the pressure fluctuation becomes relatively simple, increasing monotonically from a minimum to a maximum and then decreasing monotonically to another minimum. The amplitude of fluctuation is also reduced. These facts indicate a less dramatically changing process in a cycle. This should be due to the fact that the vortex is very small. Figure 11(b) presents the results of FFT analysis of the pressure fluctuation. The major frequency is 167.7 Hz which is exactly the cycle frequency of the blue box in Figure 11(a).

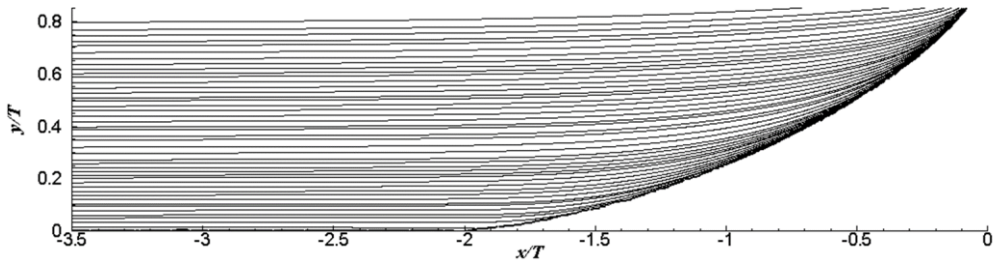

(a) Vortex system by RANS equations.

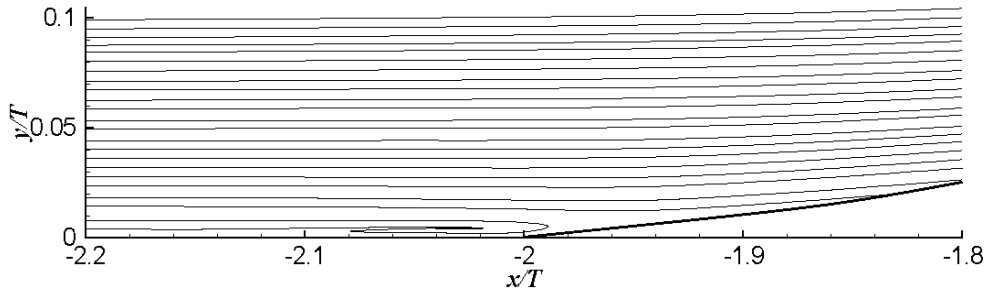

(b) Vortex system by LES, with local amplification.

Figure 10: Vortex system on the symmetric plane for the wing with a long strake.

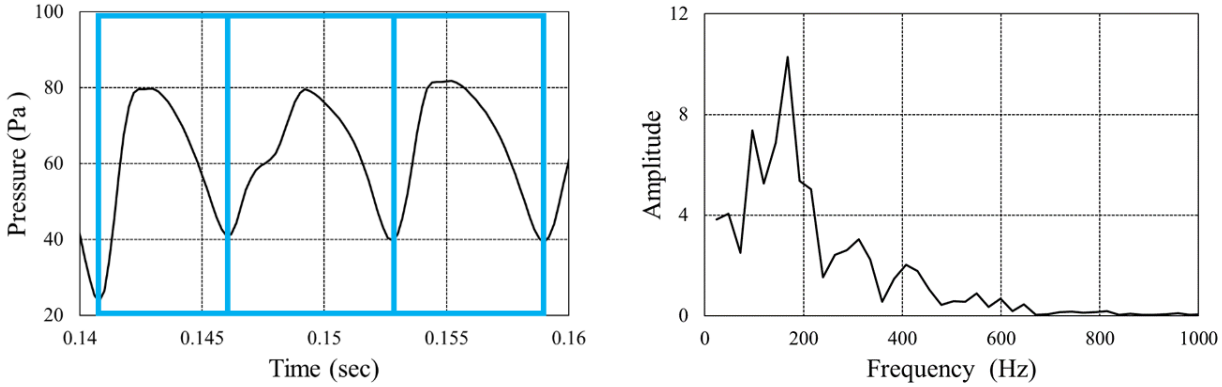

(a) Pressure variation with time.

(b) FFT analysis for the pressure.

Figure 11: Pressure fluctuation at (x/T, y/T) = (−2.036, 0.004).

The vortex development in a cycle is shown in Figure 12. It is exhibited in five stages. At stage (a), the vortex is formed upstream and moves downstream. As its center passes the observation point at (x/T, y/T) = (−2.036, 0.004), the pressure at this point reaches its minimum. As it moves further downstream and develops along the strake surface, the pressure at the observation point rises and reaches its maximum. Then a few moments later, at stage (c), a new vortex is formed upstream and moves toward the observation. Therefore, the pressure at the observation point decreases gradually. In the meantime, the vortex above the strake decays and decreases in size and deforms by shear stretching as it moves up, shown at stage (d). Finally, at stage (e), the new vortex reaches at the observation point, the vortex above the strake dies away.

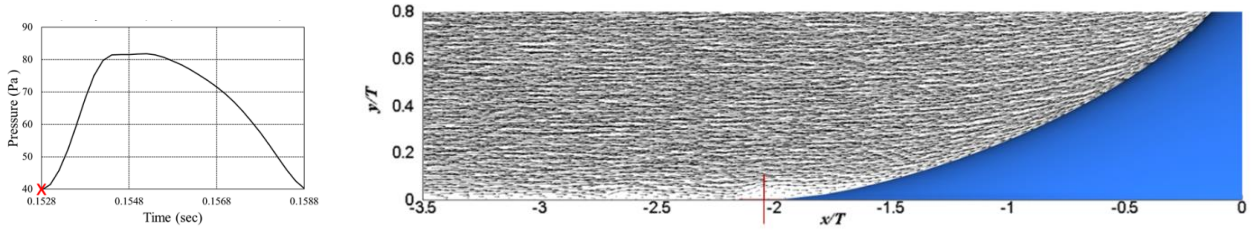

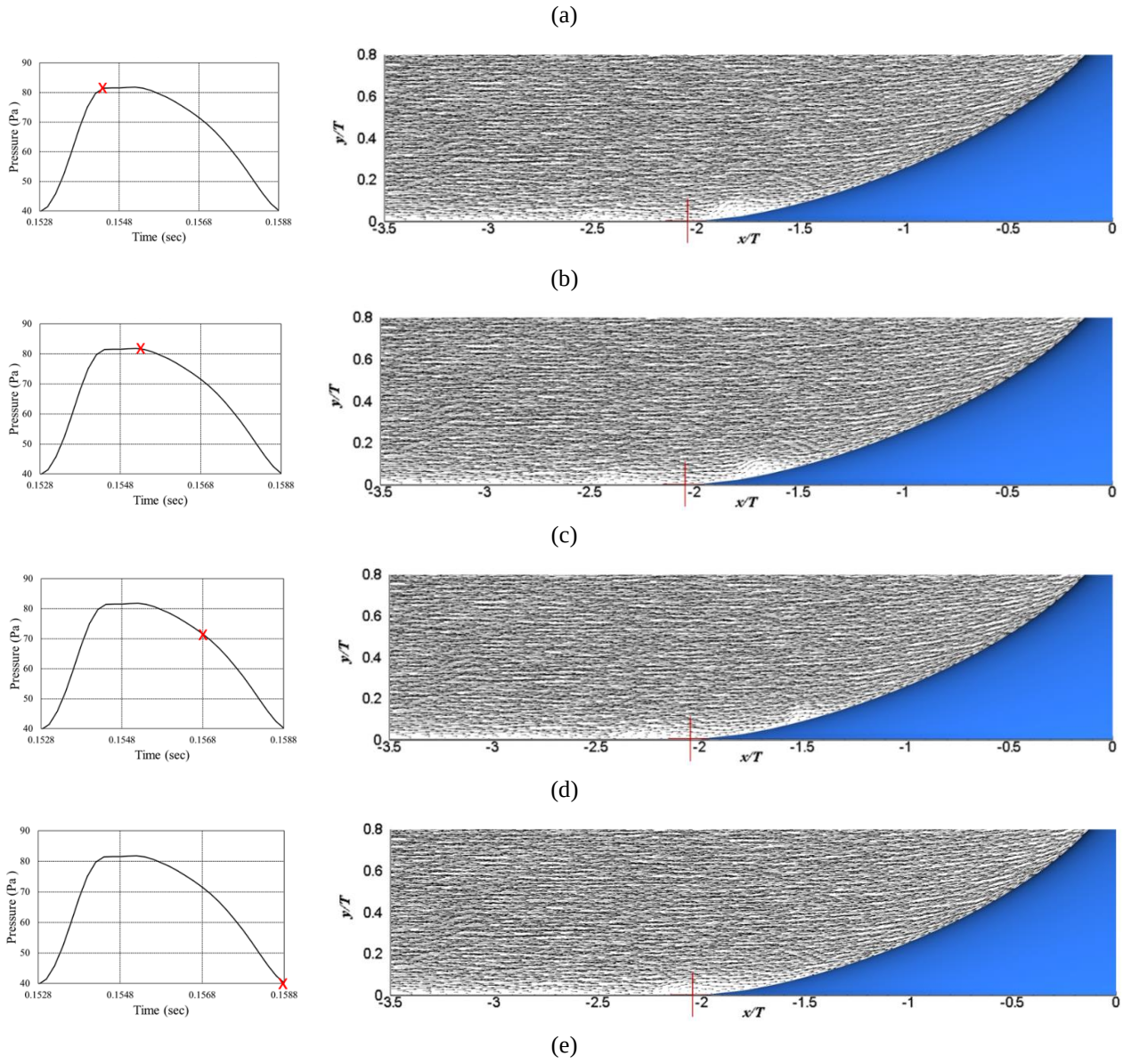

Figure 12: Motion of vortices and their amalgamation in a cycle for the wing with a long strake.

4 CONCLUSIONS

In this study, we have investigated the wing-body junction flow with a strake by RANS computations and LES. We have two purposes for this study: to understand the effect of strake designed in the present study on mitigating horseshoe vortex and to compare the results by RANS computations and LES. From the computational results, we have following observations.

The strakes designed in this study are effective to mitigate the horseshoe vortex as revealed in the computational results by both RANS and LES method. It has been known that a strake fitted to a wing in the wing-body junction flow can be an effective way to suppress the horseshoe vortex. Our study shows that the effectiveness depends on its length. For a short strake, L/T = 0.5, the horseshoe is weakened but not totally suppressed; for a long one, L/T = 2.0, the horseshoe vortex is almost suppressed. Combining other studies [19], we find that strakes of various forms can be employed to mitigate the horseshoe vortex if L/T is larger than 2.

The results by LES reveal more physical details than those by RANS. In LES computations, the unsteadiness and cycle of junction flow is well exposed in LES computations. Each cycle consists of complicated creation, amalgamation and decay of vortices. These vortices can move downstream for some time and upstream for other time. All these phenomena make the vortical flow look quite different from

those found in the RANS computations. However, if only the horseshoe vortex suppression is concerned, it appears that both RANS and LES computations agree each other. That is, RANS computation is enough to justify if the horseshoe vortex is effectively suppressed.

ACKNOWLEDGEMENTS

The authors would like to express their acknowledgements to Ministry of Science and Technology, Taiwan for supporting their research under the grant #108-2221-E-019-023.

REFERENCES

[1] Morikawa, G.K. *The wing-body problem for linearized supersonic flow*. Ph.D. dissertation, California Institute of Technology, Pasadena, CA, USA, 1949.

[2] Stanbrook, A. *Experimental observation of vortices in wing-body junctions*, ARC Technical Report, R&M No. 3114, HM Stationery Office, London, UK, 1959.

[3] Hilton, W.F. "Tests of a fairing to reduce the drag of a supersonic swept-wing root." In: *Journal of the Aeronautical Sciences*, 22, 173-178, 2955.

[4] Shabaka, I.M.M.A. and P. Bradshaw, "Turbulent flow measurements in an idealized wing/body junction." In: *AIAA Journal*, 19, 131-132, 1981.

[5] Simpson, R.L. "Junction flows." In: *Annual Review of Fluid Mechanics*, 33, 415-443, 2001.

[6] Fleming, J.L., R.L. Simpson, J.E. Cowling, and W.J. Devenport, "An experimental study of a turbulent wing-body junction and wake flow." In: *Experiments in Fluids*, 14, 366-378, 1993.

[7] Devenport, W.J. and R.L. Simpson, "Time-dependent and time-averaged turbulence structure near the nose of a wing-body junction." In; *Journal of Fluid Mechanics*, 210, 23-55, 1990.

[8] Paik, J., C. Escauriaza, and F. Sotiropoulos, "On the bimodal dynamics of the turbulent horseshoe vortex system in a wing-body junction." In: *Physics of Fluids*, 19, 045107, 2007.

[9] Gand, F., S. Deck, V. Brunet, and P. Sagut, "Flow dynamics past a simplified wing body junction." In: *Physics of Fluids*, 22, 115111, 2010.

[10] Mehta, R.D. "Effect of wing nose shape on the flow in a wing/body junction." *The Aeronautical Journal*, 88, 456-460, 1984.

[11] Ölçmen, S.M. and R.L. Simpson, "Influence of wing shapes on surface pressure fluctuations at wing-body junctions." In: *AIAA Journal*, 32, 2177-2183, 1992.

[12] Ahmed, A. and M.J. Khan, "Effects of sweep on wing-body juncture flow." In: *33rd Aerospace Sciences Meeting and Exhibit*, Reno, NV, USA, 1995.

[13] Beg, M. and S. Beg, "Scour reduction around bridge piers: a review." In: *International Journal of Engineering Inventions*, 2(7), 7-15, 2013.

[14] Devenport, W.J., N.K. Agarwal, M.B. Dewitz, R.L. Simpson, and K. Poddar, "Effects of a fillet on the flow past a wing-body junction." In: *AIAA Journal*, 28, pp. 2017-2024, 1990.

[15] Devenport, W.J., R.L. Simpson, M.B. Dewitz, and N.K. Agarwal, "Effects of a leading-edge fillet on the flow past an appendage-body junction." In: *AIAA Journal*, 30, 118-122, 1992.

[16] Wang, J.M., W.T. Bi, and Q.D. Wei, "Effects of an upstream inclined rod on the circular cylinder-flat plate junction flow." In: *Experiments in Fluids*, 46, 1093-1104, 2009.

[17] Kang, K.J., T. Kim, and S.J. Song, "Strength of horseshoe vortices around a circular cylinder with an upstream cavity." In: *Journal of Mechanical Science and Technology*, 23, 1773-1778, 2009.

[18] Theberge, M.-A. and A. Ekmekci, "Effects of an upstream triangular plate on the wing-body junction flow." In: *Physics of Fluids*, 29, 097105, 2017.

[19] Lee, J.P., J.H. Chen, and C.Y. Hsin, "Horseshoe vortex suppression with a strake." In: Rocha Á., Guarda T. (eds) *Developments and Advances in Defense and Security*. MICRADS 2018. Smart Innovation, Systems and Technologies, Vol 94. Springer, Cham, 2018.

[20] Spalart, P.R. and M.L. Shur, "On the sensitization of turbulence models to rotation and curvature." In: *Aerospace Science and Technology*, 5, 297-302, 1997.

[21] Shur, M.L., M.K. Strelets, A.K. Travin, and P.R. Spalart, "Turbulence modelling in rotation and curved channels: assessing the Spalart-Shur correction." In: *AIAA Journal*, 38, 784-792, 2000.

[22] Smagorinsky, J., "General circulation experiments with the primitive equations. I: The basic experiment." In: Monthly Weather Review, 91(3), 99-164, 1963.

[23] Lilly, D.K., "On the application of the eddy viscosity concept in the inertial subrange of turbulence." *NCAR Manuscript*, No 123, Boulder, CO, USA, 1966.

[24] Germano, M., U. Piomelli, P. Moin, and W.H. Cabot, "Dynamic subgrid-scale eddy viscosity model." In: *Summer Workshop, Center for Turbulence Research*, Stanford, CA, USA, 1996.

[25] Lilly, D.K., "A proposed modification for the Germano subgrid-scale closure model." In: *Physics of Fluids*, 4, 633-635, 1992.

[26] Devenport, W.J. and R.L. Simpson, *An Experimental Investigation of the Flow past an Idealized Wing-Body Junction: Data Report*. Dept. of Aerospace and Ocean Engineering, Virginia Polytechnic Institute and State University, 1987.